Complementary Three-Dimensional Quantitative Structure−Activity Relationship Modeling of Binding Affinity and Functional Potency: A Study on $\alpha_4\beta_2$ Nicotinic Ligands

Paolo Tosco,[†] Philip K. Ahring,[‡] Tino Dyhring,[‡] Dan Peters,[‡] Kasper Harpsøe,[§] Tommy Liljefors,[§] and Thomas Balle*[,§]

Department of Drug Science and Technology, University of Turin, Via Pietro Giuria 9, 10125 Torino, Italy, Drug Discovery, NeuroSearch A/S, 93 Pederstrupvej, DK-2750 Ballerup, Denmark, Department of Medicinal Chemistry, The Faculty of Pharmaceutical Sciences, University of Copenhagen, 2 Universitetsparken, 2100 Copenhagen, Denmark

Received August 25, 2008

Complementary 3D-QSAR modeling of binding affinity and functional potency is proposed as a tool to pinpoint the molecular features of the ligands, and the corresponding amino acids in the receptor, responsible for high affinity binding vs those driving agonist behavior and receptor activation. This approach proved successful on a series of nicotinic $\alpha_4\beta_2$ ligands, whose partial/full agonist profile could be linked to the size of the scaffold as well as to the nature of the substituents.

Introduction

Ligand binding to a receptor is necessary but not sufficient for a functional response, and development of small molecule agonists in medicinal chemistry is often hampered by the fact that even minor modifications of a promising agonist scaffold lead to decrease or even loss of functional potency and intrinsic activity. Binding affinities (IC_{50} values), functional potencies (EC_{50} values), and intrinsic activities (% maximal response relative to a reference) each contribute to characterize ligand recognition and receptor activation processes. Information about the capacity of a ligand to bind and possibly to activate a receptor at a molecular level is inherent in the 3D[a] structure of its bioactive conformation. Having both binding affinities and functional potencies at hand for a properly selected set of ligands, it should in principle be possible to extract such information with 3D-QSAR techniques. This methodology has extensively been used to optimize and understand structure−affinity as well as structure−activity relationships. However, the combination of multiple QSAR models to pinpoint the structural features of the ligands and the corresponding amino acid partners in the receptor responsible for binding vs those driving agonist/antagonist behavior has not previously been described.

In a previous work[1] we reported a 3D-QSAR study on a series of ligands with affinity for the $\alpha_4\beta_2$ subtype of nicotinic receptors. Because of the remarkable diversity of this data set both in the bicyclic scaffold and in the substituents at the pyridine ring, it was possible to generate GRID/GOLPE models[2,3] of high quality and interpretability. Analysis of the isocontours on 3D coefficient plots revealed the favorable impact on affinity of increasing the size of the ring system bearing the protonated nitrogen as well as the importance of effective charge-enhanced hydrogen bonding of the latter. Putative acceptors in the active site were identified to be Trp147 and Tyr91 (α_4 subunit), on the basis of a homology model developed by Le Novere et al.[4] Because this series of compounds appeared very promising, compounds were further characterized in in vitro functional assays. Then, prompted by the success of the 3D-QSAR analysis based on [^{3}H]-cytisine binding data, we attempted to build another model using functional potencies. Our goal was to investigate if it is possible to combine the information from binding affinity- and functional potency-based 3D-QSAR models to gain insight in the structural motifs that influence binding and functional behavior at the $\alpha_4\beta_2$ receptors. Herein we present the results of our investigation.

Chart 1. Structures of Compounds **1**−**36**[a]

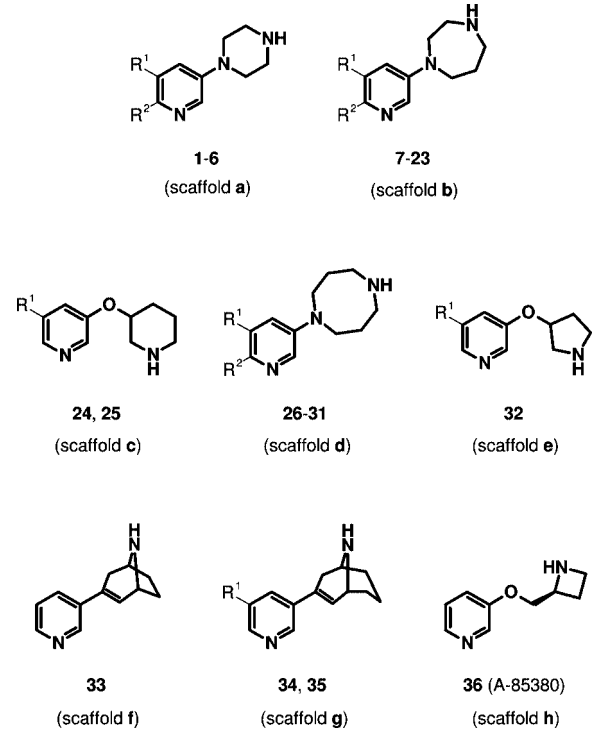

[a] Scaffolds **a**−**h** are evidenced with thicker lines.

Results and Discussion

Pharmacology. The 56 compounds making up the original data set[1] were tested for agonist activity at human $\alpha_4\beta_2$ receptors

* To whom correspondence should be addressed. Phone: +45-353-36409. Fax: +45-353-36001. E-mail: tb@farma.ku.dk.
[†] Department of Drug Science and Technology, University of Turin.
[‡] Drug Discovery, NeuroSearch A/S.
[§] Department of Medicinal Chemistry, The Faculty of Pharmaceutical Sciences, University of Copenhagen.

[a] Abbreviations: 3D, three-dimensional; QSAR, quantitative structure−activity relationship; PLS, partial least-squares; QMD, quenched molecular dynamics; PC, principal component; SDEP, standard deviation of the error of prediction.

10.1021/jm801060h CCC: $40.75
Published on Web 03/20/2009

Table 1. Binding Affinities, Functional Potencies, and Intrinsic Activities of Compounds **1**−**36**

compd	R^1	R^2	pIC_{50} (obsd)[a]	pIC_{50} (pred)	pEC_{50} (obsd)[b]	pEC_{50} (pred)	efficacy (% of max)[c]
1	$OCH{=}CH_2$	H	6.72	6.82[d]	5.12	5.34[d]	18
2	OCH_3	Br	6.74	6.71[d]	4.77	4.82[d]	68
3	Br	Cl	6.64	6.61[d]	5.10	4.69[d]	98
4	Cl	CH_3	6.28	6.44[d]	4.57	4.75[d]	74
5	Cl	H	6.51	6.49[e]	4.64	5.31[e]	41
6	H	Br	6.74	6.58[d]	5.60	5.04[d]	129
7	*cis*-$OCH{=}CHCH_3$	H	8.89	8.77[d]	5.68	5.75[d]	45
8	Cl	Br	8.85	8.62[e]	7.82	6.85[e]	102
9	Br	Cl	8.85	8.86[d]	7.24	6.96[d]	85
10	OH	I	7.66	7.96[d]	6.32	6.35[d]	104
11	$OCH{=}CH_2$	H	8.30	8.80[e]	5.96	6.48[e]	61
12	$CONH_2$	H	7.70	7.85[d]	4.89	5.36[d]	56
13	OH	H	8.62	8.19[d]	6.85	6.62[d]	120
14	OCH_3	H	8.72	8.40[d]	5.85	5.31[d]	66
15	H	Br	9.00	8.73[d]	7.19	6.95[d]	88
16	H	SCH_2CH_3	6.77	6.84[d]	5.35	4.96[d]	53
17	H	OCH_3	6.77	7.14[e]	4.96	5.58[e]	88
18	OCH_2CH_3	Br	9.06	9.12[d]	6.59	6.73[d]	78
19	OCH_3	Cl	9.17	9.08[d]	7.04	7.29[d]	116
20	quinoline		8.18	8.71[d]	5.44	5.56[d]	33
21	$OCH{=}CH_2$	Br	9.19	9.15[d]	6.96	6.86[d]	80
22	$OCH_2CH_2OCH_3$	H	8.62	8.68[d]	5.06	5.15[d]	42
23	H	H	8.72	8.36[e]	6.64	6.45[e]	94
24	Cl	H	6.62	6.58[d]	5.85	5.72[d]	15
25	H	H	6.72	6.66[e]	4.49	5.76[e]	22
26	OCH_3	H	9.00	8.85[d]	6.92	6.82[d]	89
27	H	H	9.05	8.78[e]	7.44	7.03[e]	78
28	H	Br	9.35	9.29[d]	8.89	8.08[d]	139
29	Cl	H	8.70	8.69[e]	6.77	6.98[e]	103
30	$OCH{=}CH_2$	Br	9.42	9.66[d]	6.62	7.47[d]	90
31	Br	H	8.55	8.74[d]	6.74	6.96[d]	73
32	H	H	7.00	6.96[d]	4.54	5.00[d]	54
33	H	H	8.17	8.28[d]	6.00	6.31[d]	66
34	H	H	8.35	7.94[e]	5.92	6.34[e]	34
35	OCH_3	H	8.52	8.43[d]	5.36	5.45[d]	13
36			8.82	8.70[d]	6.15[f]	6.01[d]	183

[a] Determined as inhibition of [^{3}H]-cytisine binding.[1] [b] Determined by a calcium-based functional assay (FLIPR) using a HEK-293 cell line stably expressing human $\alpha_4\beta_2$ nicotinic receptors; SD < 0.3 ($n = 4-8$). [c] Maximum agonist activity is normalized relative to 100 μM (−)-nicotine. [d] Recalculated value; the compound belongs to the training set. [e] Predicted value; the compound belongs to the test set. [f] Data from Sullivan et al., 1996 (ref 14).

in a functional fluorescence-based assay to establish functional potency and efficacy values relative to (−)-nicotine. However, for a number of compounds, it was not possible to detect significant functional activity. These compounds might either be antagonists or have too partial an agonist activity to be detected in the assay. Therefore, the data set was reduced to 36 compounds (**1**−**36**, Chart 1, Table 1) because including molecules which cannot be attributed a precise pEC_{50} value could potentially bias the model.

3D-QSAR Analysis. Our investigation started from the observation that 57% of the variance in functional potency (expressed as pEC_{50}) is accounted for by the variance in binding affinity (expressed as pIC_{50}) (plot reported in Supporting Information). Although the two properties are correlated, a substantial amount of variation in the functional potency data is not accounted for by binding affinity. Therefore, a simple prediction of functional potency on the basis of binding affinity could lead to severe misinterpretations, as evident for instance in the case of compound **22** (Table 1), for which the two values differ by more than 3 orders of magnitude. The significant fraction of unexplained variance suggests that a PLS analysis based on GRID energy maps might yield different models using as dependent variables binding affinities or functional potencies, respectively. To test this hypothesis, at first we built a model using the same superposition scheme adopted previously[1] based on the best alignment of five fitting points (pyridine nitrogen, pyridine centroid, protonated nitrogen on the alicyclic ring system, and the two hydrogens connected to the latter) onto compound **23**, chosen as a template. The robustness of the previous model[1] was confirmed because reduction to 36 compounds in the training set still yielded excellent statistics ($r^2 = 0.92$, leave-20%-out $q^2 = 0.82$). However, less satisfactory results were obtained by correlating the calculated GRID energies to the functional potency of the compounds ($r^2 = 0.80$, leave-20%-out $q^2 = 0.44$). Before concluding that a clear correlation between GRID energy maps and functional potency does not exist for the present data set, we reconsidered our superposition protocol because the dependency of 3D-QSAR models on the alignment of compounds is a well-known issue.[5] While we trusted the five-fitting-point scheme, which relies upon solid SAR and proved successful in the past,[1,6] we turned our attention to other aspects. In our previous work, we explored the conformational space of ligands by means of a stochastic conformational search. To rule out the possibility that we might have missed low-energy conformers due to the limits of certain implementations of the Monte Carlo method in sampling cyclic systems,[7] we decided to repeat the conformational search using high-temperature QMD,[8] keeping all conformations in a 1 kcal span from the global minimum. Additionally, we reasoned that the choice of an arbitrary stable conformer of compound **23** as the template for superposition might not be optimal. To this purpose, we thoroughly analyzed our data set; after removing

Table 2. 3D-QSAR Models Obtained Using Different Templates for the Alignment[a]

model	ranking[b]	r^2 (pIC_{50})[c]	SDEP (pIC_{50})[d]	r^2 (pEC_{50})[e]	SDEP (pEC_{50})[f]
e2	1	0.96	0.30 (1)	0.88	0.68 (2)
h3	2	0.95	0.35 (5)	0.83	0.67 (1)
e3	3	0.92	0.34 (3)	0.83	0.73 (4)
c1	4	0.95	0.36 (8)	0.86	0.74 (5)
f2	5	0.96	0.40 (12)	0.86	0.74 (5)
f1	6	0.94	0.34 (3)	0.81	0.81 (16)
g2	7	0.96	0.38 (10)	0.82	0.77 (10)
f3	8	0.97	0.37 (9)	0.85	0.79 (12)
g4	9	0.94	0.35 (5)	0.82	0.82 (17)
h2	9	0.94	0.30 (1)	0.84	0.88 (21)
a1	11	0.96	0.44 (16)	0.80	0.75 (7)
b3	11	0.92	0.38 (10)	0.82	0.80 (13)
f4	11	0.94	0.35 (5)	0.82	0.83 (18)
g1	14	0.96	0.40 (12)	0.85	0.80 (13)
g3	14	0.96	0.43 (15)	0.86	0.77 (10)
c3	14	0.90	0.55 (22)	0.83	0.69 (3)
e1	17	0.95	0.48 (19)	0.82	0.75 (7)
c2	18	0.94	0.52 (20)	0.89	0.76 (9)
a2	19	0.97	0.45 (18)	0.85	0.80 (13)
b4	20	0.91	0.44 (16)	0.85	0.88 (21)
b1	21	0.95	0.40 (12)	0.85	0.99 (29)
reference[g]		0.93	0.45	0.81	0.90
e4	22	0.94	0.56 (23)	0.85	0.87 (19)
b2	23	0.93	0.59 (24)	0.90	0.87 (19)
d1	24	0.96	0.64 (27)	0.87	0.88 (21)
h4	24	0.94	0.54 (21)	0.84	0.93 (27)
d2	26	0.94	0.59 (24)	0.91	0.92 (25)
d4	27	0.92	0.59 (24)	0.85	0.93 (27)
d3	28	0.95	0.77 (29)	0.88	0.91 (24)
h1	28	0.94	0.67 (28)	0.83	0.92 (25)

[a] Training set: 27 compounds; test set: 9 compounds. Models have been labeled by a code that identifies the template used for the alignment; the letter indicates the scaffold type (see Chart 1), while the number identifies a particular low-energy conformer available to all members of that family. [b] Absolute ranking of the model based on its combined predictive performances of binding affinity and functional potency, respectively. [c] Value of r^2 for the 27-compound model based on pIC_{50} values. [d] Value of SDEP of pIC_{50} values for test set compounds; the relative ranking of the model is reported within parentheses. [e] Value of r^2 for the 27-compound model based on pEC_{50} values. [f] Value of SDEP of pEC_{50} values for test set compounds; the relative ranking of the model is reported within parentheses. [g] Alignment used in the previously obtained model,[1] included as a reference.

all substituents (which are not taken into consideration by the alignment protocol), we identified eight different scaffold families (**a**−**h**, thicker drawing in Chart 1). Because the torsional angle between the two rings can assume different values and the alicyclic ring systems have a certain intrinsic flexibility, especially the larger ones, each of these scaffolds may exist in different conformations. Interestingly, it was noticed that certain scaffold conformations are consistently found in all members of each family, proving that certain low-energy conformations of these bicyclic scaffolds are largely independent of the substituents at the pyridine ring. Overall, 29 of these ubiquitous scaffold conformations were found that could act as templates for the alignment of ligands according to the five fitting points mentioned above. Two GRID/GOLPE models were generated for each of the 29 templates as described in the Experimental Section, one based on binding affinity and the other on functional potency. To set a robust criterion for scoring the quality of obtained models, the data set was split into a 27-compound training set and a 9-compound test set; left-out compounds (**5**, **8**, **11**, **17**, **23**, **25**, **27**, **29**, **34**) where chosen among the scaffold families that have multiple members. Models were classified according to their combined ranking in terms of predictive performance, assessed by the SDEP of the test set compounds activities. This criterion identifies the models that are successful both in predicting affinity and functional potency, ruling out those that have less good or unbalanced performance. The individual SDEP values for the 29 pairs of models with 3 PCs using a methyl (C3) and a water (OH2) probe are collected in Table 2; the results obtained in the same conditions using the previously reported alignment[1] have been included for comparison. The consistency of this scoring criterion can be appreciated by the fact that the four best models are characterized by good, balanced performance with either set of dependent variables. The average SDEP of pEC_{50} values is almost double than the one of pIC_{50} values (0.82 vs 0.42), which probably reflects the intrinsically more noisy nature of functional data compared to binding affinities and their less tight connection with GRID energy variables. Overall, the **e2** alignment generated the best model, characterized by SDEPs of 0.30 and 0.68 for pIC_{50} and pEC_{50} values, respectively. Because this alignment is supported by two predictive 3D-QSAR models, whose dependent variables are only weakly correlated, as discussed earlier, it can be envisaged to be a reasonable guess of the bioactive conformation. The most evident difference between the best scoring superposition schemes and the others lies in the alignment of the R^1 substituents at the pyridine nucleus: compared to the best-scoring model **e2**, in the superpositions arising from the **b** and **d** templates, the R^1 substituents are much less consistently aligned. This is due to the fact that ligands bearing the smallest, less flexible rings (mostly piperidines and piperazines), in the attempt to stretch and cover the larger distance that separates the protonated nitrogen from the pyridine nitrogen in the larger **b** and **d** templates (azepane or azocane, respectively), as a side effect scatter their substituents over a wide angle, yielding noisy models endowed with lower predictive power. The degree of steric and electrostatic complementarity of the **e2** alignment with the active site was examined using a new, in-house homology model of the $\alpha_4\beta_2$ dimer interface.[9] To this purpose, a full 36-compound model was built by merging training and test sets (pIC_{50} model: $r^2 = 0.94$, leave-20%-out $q^2 = 0.86$; pEC_{50} model: $r^2 = 0.87$, leave-20%-out $q^2 = 0.59$). Subsequently, the ensemble of 36 superposed ligands

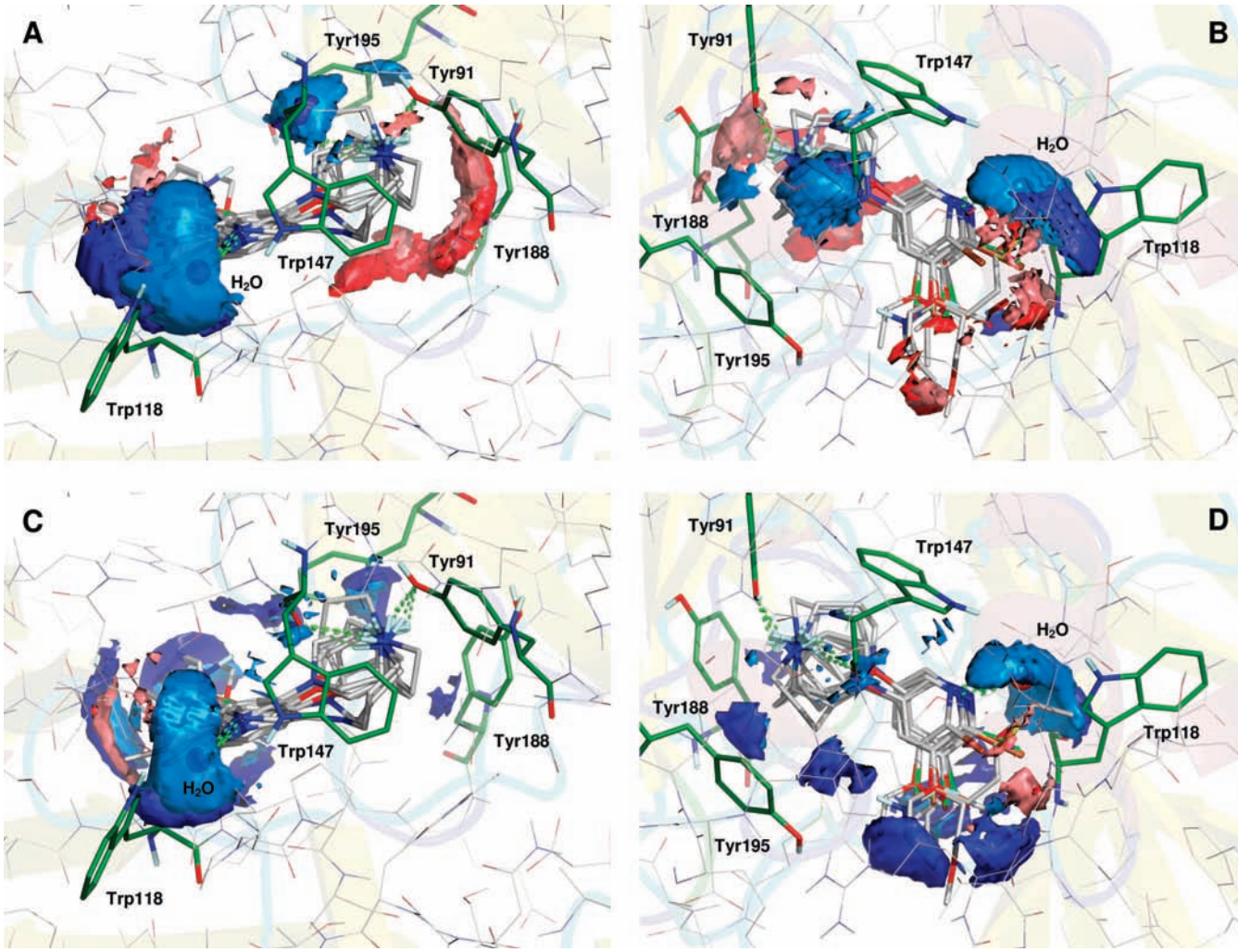

Figure 1. The **e2** conformer ensemble of compounds **1**−**36** in the $\alpha_4\beta_2$ binding cavity. Positive isocontours are depicted in red, negative in blue. Darker colors are used for the C3 probe, lighter for the OH2 probe. Side view (A) and top view (B) for the binding affinity model (isocontour level $\pm 3.75 \times 10^{-4}$). Side view (C) and top view (D) for the functional potency model (isocontour level $\pm 2.50 \times 10^{-4}$).

that constitute model **e2** was rigidly docked as a whole in the cleft between subunits α_4 and β_2, using as a guide the experimental binding mode found for nicotine[10] and epibatidine[11] in the binding site of AChBP. Parts A and B of Figure 1 show the isocontours for the 36-compound model based on binding affinity, while parts C and D of Figure 1 display those for the model based on functional potencies. Isocontours show the grid points where PLS coefficients assume a value higher than a certain threshold in absolute value, which is the zone where the dependent variable (i.e., affinity or functional potency) is more strongly correlated with independent variables (i.e., GRID energies). Generally speaking, in C3 probe maps, large positive coefficients identify areas where steric bulk favors affinity (or functional potency), while negative coefficients appear where steric hindrance is detrimental to affinity (or functional potency). In OH2 probe maps, negative coefficients show up where a hydrogen bond is likely to form because the establishing of such interactions reduces overall potential energy. However, a word of caution is needed in interpreting OH2 probe isocontours because this probe is not purely electrostatic in its nature (like, for example, the point charge used in CoMFA), but it contains a steric component due to the van der Waals volumes of oxygen and hydrogen atoms. Therefore, the sign and magnitude of the coefficients may reflect a combination of electrostatic and steric effects. Figure 1 shows that all compounds with good affinity for the $\alpha_4\beta_2$ active site establish hydrogen bonds with the Trp147 backbone carbonyl oxygen as well as with the Tyr91 hydroxyl group. Because of the smaller size of the ring, the piperazines **1**−**6**, as well as the piperidines **24** and **25**, are less flexible; therefore, they cannot assume a low-energy conformation that puts the two hydrogens connected to the basic nitrogen in a correct geometry for hydrogen bonding. All ligands form a hydrogen bond interaction between their pyridine nitrogen and a conserved water molecule; the latter is consistently present in all interfaces between subunits in the crystal structure of nicotine−AChBP complex,[10] and was therefore included in our homology model. These findings confirm those presented in our former work.[1] Furthermore, comparison with the earlier model shows that the collocation of the ligands with respect to each other is very similar in the two models. The main difference lies in the overall arrangement of the protonated ring with respect to the pyridine nucleus; actually, the two moieties assume partially specular conformations in the two models (see Figure 2). While both the old and the new model fit the receptor, the new one seems to establish more efficient hydrogen bonds with the Trp147 backbone carbonyl oxygen, especially with the most potent azepane and azocane agonists. It is not surprising that the two models, although in some respect similar, have quite different performances. It is evident that large clusters of grid points, namely

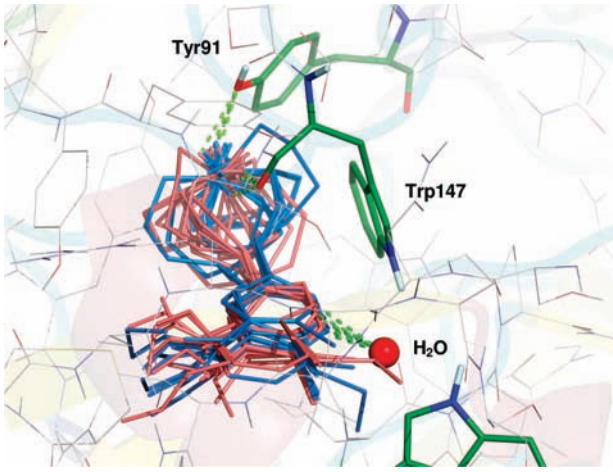

Figure 2. Comparison between the alignment obtained in our previous work[1] (in blue) and in the present one (in red). While the reciprocal arrangement of the ligands is very similar in the two models, the protonated ring as well as the pyridine substituents assume partially specular conformations; in particular, the different orientation of the hydrogens connected to the protonated nitrogen seems to favor hydrogen bonding to Trp147.

those related to the side chain and to the protonated ring, are necessarily characterized by very similar energy values in the two models. However, while 3D-QSAR models treat energy values as a linear array, largely neglecting their original collocation in the three-dimensional grid, the Smart Region Definition (SRD) algorithm implemented in GOLPE clusters grid points that are close in space so that also the reciprocal collocation of energy values in the Cartesian space gains much importance. In our opinion, this is the main reason of the better performance of the new model compared to the old one. Furthermore, the comparison between the coefficient plots of the affinity and activity-based models suggests a number of interesting considerations. In both models, the negative contour in proximity to the pyridine nitrogen is generated predominantly by the OH2 probe, while the small contribution from the C3 probe simply reflects a steric clash of some compounds with the Trp118 residue in the β_2 subunit. This indicates that hydrogen bonding to the conserved water molecule is a requisite both for binding and for agonistic activity. Hydrogen bonding from the protonated basic nitrogen to both Trp147 and Tyr91 appears to be critical to achieve good affinity, while in the pEC_{50} model, a small but well-defined contour generated by the OH2 probe only appears in proximity to Trp147. Other significant differences between pIC_{50} and pEC_{50} contours lie in the volumes occupied by pyridine substituents and by the protonated ring. In the binding data model, positive contours are generated by both probes near the larger R^1 substituents (Chart 1), which suggests that these contours are purely steric in nature. The latter become negative when the functional potency model is considered: this represents a very important indication of a possible role of R^1 substituents in shifting the pharmacological profile from agonism to partial agonism and possibly antagonism. On the contrary, positive contours appear when R^2 (Chart 1) is a halogen, which suggests a positive influence on agonistic behavior, while binding seems to be slightly less influenced. A well-defined, positive steric contour lining Tyr188 and the C-loop cysteine bridge is generated by both probes in the pIC_{50} model. A similar contour, this time negative, appears in the functional data model. An additional negative steric contour arises in proximity of Tyr195. The indication that increasing the size of the protonated ring has favorable impact on affinity had already emerged from our previous model;[1] the new results stress the role played by Tyr188 and Tyr195 as the "lid" of the active site. It is known from the crystal structure of AChBP in complex with α-conotoxin that bulky antagonists can induce the outward displacement of the C-loop region,[12] to which Tyr188 and Tyr195 are directly connected. Our results suggest that these latter residues can actually move quite freely in response to increased size of the ligands, which explains the excellent binding affinity of bulky ligands and the large positive contours in the pIC_{50} model but at the cost of impairing the capacity to activate the receptor. Further studies are needed to address whether the larger R^1 substituents at the pyridine ring may trigger a similar effect by a different route.

Conclusions

A functional in vitro pharmacological characterization has been carried out on a series of previously published ligands with affinity for the $\alpha_4\beta_2$ nicotinic receptor subtype. Taking advantage of the new data, a combined 3D-QSAR study has been undertaken by building two models, one based on binding affinity and one on functional potency. A strategy of SDEP-driven conformational sampling has been successfully applied to find the best alignment of compounds, one of the most crucial aspects in 3D-QSAR modeling. While confirming our previous findings, the new superposition scheme has notably improved the predictive performance of the model based on new functional potency data with respect to the alignment used in our former work. In particular, a possible role emerged for the substituents at the pyridine ring, which seem to control the degree of $\alpha_4\beta_2$ receptor efficacy. Also the size of the ring bearing the protonated nitrogen appears to modulate agonism; the possibility that its interaction with Tyr188 and Tyr195 may trigger to some degree the same displacement of the C-loop as experimentally observed for α-conotoxin deserves further investigation. The structural features which make a good binder an equally good agonist are often elusive; in this respect, combining the information provided by two largely orthogonal 3D-QSAR models yielded useful insight on the moieties involved in $\alpha_4\beta_2$ receptor activation.

Experimental Section

Purity data for compounds **1**−**36** are available in previous publications.[1,6]

Cell Culture. The human nAChR α_4 and β_2 subunits were cloned from the IMR32 cell line as described previously.[13] A HEK-293 cell line stably expressing h$\alpha_4\beta_2$ was propagated in Dulbecco's modified Eagle's medium (Gibco) containing 10% fetal bovine serum (Gibco) at 37 °C in a humidified atmosphere containing 5% CO_2.

Intracellular Calcium-Based Functional Assay. HEK-h$\alpha_4\beta_2$ cells were seeded on poly-D-lysine-coated 96-well microtiter plates (Corning Inc.) and were allowed to proliferate for 24 h. Dye loading was performed by incubating cells with 2 μM fluo-4/AM (InVitrogen) for 1.5 h at room temperature. Dye not taken up by cells was removed by aspiration, followed by three washing cycles with NMDG Ringer buffer (100 μL; in mM: 140 NMDG, 5 KCl, 1 $MgCl_2$, 10 $CaCl_2$, 10 HEPES, pH 7.4), after which the cells were kept in the same buffer (100 μL). The microtiter plates were placed in a FLuorimetric Imaging Plate Reader (FLIPR, MDS Analytical Technologies) and subjected to test compounds **1**−**35** (100 pM to 100 μM). Background-subtracted compound-mediated calcium responses were normalized to (−)-nicotine (100 μM) control responses and pEC_{50}, as well as relative maximal efficacy values, were determined. The activity of compound **36** has been previously assessed.[14]

Conformational Search. Molecular models of compounds **1**−**36** were constructed in their *N*-protonated form using standard bond lengths and angles with the MOE software package.[15] Their

geometries were optimized with the MMFF94s force field using a truncated Newton−Raphson algorithm until the gradient was lower than 0.01 kcal mol^{-1}; the solvent was modeled as a continuum by the GB/SA method. On each structure, a conformational search by QMD was carried out with CHARMM[16] (MMFF94 force field, GB/SA implicit solvent model, no cutoff for nonbonded interactions). Two hundred high temperature (1000 K, Nosè−Hoover thermostat as implemented in CHARMM) 10 ps MD runs (time step 1 fs) were accomplished, followed by energy minimization (MMFF94s force field, 0.01 kcal mol^{-1} rms gradient termination criterion); the optimized geometry was stored in a database and used as the starting geometry for the following QMD cycle, initializing the seed for random velocity assignment before each run. The whole QMD procedure was repeated five times with different starting geometries, obtaining substantially identical results, indicating thorough sampling of the conformational space. Duplicate conformers (rmsd < 0.01, computed by keeping into account ring symmetry in 6- and 8-membered alicyclic ring systems) were eliminated from each database, as well as all conformers whose potential energy was higher than 1 kcal over the global minimum.

Superposition Procedure. Analyzing all conformations found by QMD for the 27 compounds belonging to the training set, a total of 29 possible different localizations in space were found for the collection of five fitting points previously identified (see Results and Discussion), which were available to all members of the respective scaffold family, thus leading to 29 different superposition templates. For each compound, every conformer in a 1 kcal range from the global minimum was aligned onto the template according to the five fitting points. Because no fitting point is present between the pyridine ring and the basic nitrogen, "flipped" poses could arise, which would have obvious clashes with amino acids lining the cavity and would break all known SAR. To rule out this possibility, the following condition was imposed: only conformers in which the centroid of the two protons connected to the basic nitrogen lies above a horizontal plane passing through the nitrogen itself were considered. The most stable conformer having a rmsd lower than 0.1 Å from the template was chosen from the database. For compounds existing as enantiomeric pairs, because pharmacological assays were accomplished on racemic mixtures, the best fitting enantiomer was chosen. This procedure, carried out in MOE with custom SVL scripts, yielded 29 molecular databases, each made up by 36 ligands aligned onto a different template. Their coordinates were exported to compute GRID energy maps.

GRID/GOLPE Model Building. The ligands belonging to each of the 29 databases were loaded into GRID[2] and embedded in a grid box exceeding the largest compound by 5 Å in each direction. The grid step size was set to 0.33 Å, and a dielectric constant of 4 was chosen in order to mimic the buried core of the $\alpha_4\beta_2$ dimer interface where ligands bind. The grid contours obtained using C3 (methyl) and OH2 (water) probes were imported into GOLPE[3] to build two QSAR models, one based on binding affinity and the other on functional potency. A preliminary variable reduction was carried out by zeroing energy variables below 0.05 in absolute value; variables with a standard deviation lower than 0.10 were excluded, as well as second, third, and fourth level variables. Block unweighted scaling was applied to the blocks of data corresponding to each probe. After such pretreatment, variables were grouped according to the SRD procedure[17] using the number of seeds suggested by GOLPE. Variables nearer than 0.33 Å in the space of PLS weights were grouped under the same seed and neighboring groups nearer than 0.66 Å were collapsed into a single group. Finally, FFD variable selection was applied on SRD-generated groups, including 20% dummy variables; only groups improving predictivity more than the average of dummy variables were retained. The robustness of models was finally assessed by the SDEP of test set compound affinities and activities using 3 PCs.

Acknowledgment. Part of the molecular modelling work was carried out by P.T. during a stay (funded by Italian MIUR, InterLink 2004−2006) at the Department of Medicinal Chemistry, The Faculty of Pharmaceutical Sciences, University of Copenhagen. We gratefully acknowledge the ShareGrid management team for the computing power provided through the ShareGrid distributed platform.[18] T.B. was supported by grants from the Carlsberg Foundation and the Lundbeck Foundation. K.H. was supported by a post doctoral grant from the Drug Research Academy, The Faculty of Pharmaceutical Sciences, University of Copenhagen.

Supporting Information Available: Plot of the correlation between binding affinities and functional potencies. Observed vs predicted plots for pIC_{50} and pEC_{50} values for model **e2**. This material is available free of charge via the Internet at http://pubs.acs.org.

References

(1) Audouze, K.; Nielsen, E. O.; Olsen, G. M.; Ahring, P.; Jorgensen, T. D.; Peters, D.; Liljefors, T.; Balle, T. New ligands with affinity for the $\alpha_4\beta_2$ subtype of nicotinic acetylcholine receptors. Synthesis, receptor binding, and 3D-QSAR modeling. *J. Med. Chem.* **2006**, *49*, 3159–3171.

(2) *GRID* version 22A; Molecular Discovery Ltd.: Oxford, England, 2004.

(3) *GOLPE*, version 4.5.12; Multivariate Infometric Analysis (MIA): Perugia, Italy, 2002.

(4) Le Novere, N.; Grutter, T.; Changeux, J.-P. Models of the extracellular domain of the nicotinic receptors and of agonist and Ca^{2+} binding sites. *Proc. Natl. Acad. Sci. U.S.A.* **2002**, *99*, 3210–3215.

(5) (a) Lemmen, C.; Lengauer, T. Computational methods for the structural alignment of molecules. *J. Comput.-Aided. Mol. Des.* **2000**, *14*, 215–232. (b) Pastor, M.; Cruciani, G.; McLay, I.; Pickett, S.; Clementi, S. GRid-INdependent descriptors (GRIND): a novel class of alignment-independent three-dimensional molecular descriptors. *J. Med. Chem.* **2000**, *43*, 3233–3243.

(6) Nielsen, S. F.; Nielsen, E. O.; Olsen, G. M.; Liljefors, T.; Peters, D. Novel potent ligands for the central nicotinic acetylcholine receptor: synthesis, receptor binding, and 3D-QSAR analysis. *J. Med. Chem.* **2000**, *43*, 2217–2226.

(7) Wang, C.-S. Efficient algorithm for conformational search of macrocyclic molecules. *J. Comput. Chem.* **1997**, *18*, 277–289.

(8) Altomare, C.; Cellamare, S.; Carotti, A.; Casini, G.; Ferappi, M.; Gavuzzo, E.; Mazza, F.; Carrupt, P.-A.; Gaillard, P.; Testa, B. X-Ray crystal structure, partitioning behaviour, and molecular modeling study of piracetam-type nootropics: insights into the pharmacophore. *J. Med. Chem.* **1995**, *38*, 170–179.

(9) Harpsøe, K.; Balle, T. Unpublished results, 2008.

(10) Celie, P. H. N.; van Rossum-Fikkert, S. E.; van Dijk, W. J.; Brejc, K.; Smit, A. B.; Sixma, T. K. Nicotine and carbamylcholine binding to nicotinic acetylcholine receptors studied in AChBP crystal structures. *Neuron* **2004**, *41*, 907–914.

(11) Bourne, Y.; Talley, T. T.; Hansen, S. B.; Taylor, P.; Marchot, P. Crystal structure of a Cbtx-AChBP complex reveals essential interactions between snake alpha-neurotoxins and nicotinic receptors. *EMBO J.* **2005**, *24*, 1512–1522.

(12) Ulens, C.; Hogg, R. C.; Celie, P. H.; Bertrand, D.; Tsetlin, V.; Smit, A. B.; Sixma, T. K. Structural determinants of selective α-conotoxin binding to a nicotinic acetylcholine receptor homolog AChBP. *Proc. Natl. Acad. Sci. U.S.A.* **2006**, *103*, 3615–3620.

(13) Timmermann, D. B.; Halvard Grønlien, J.; Kohlhaas, K. L.; Nielsen, E. Ø.; Dam, E.; Jørgensen, T. D.; Ahring, P. K.; Peters, D.; Holst, D.; Christensen, J. K.; Malysz, J.; Briggs, C. A.; Gopalakrishnan, M.; Olsen, G. M. An allosteric modulator of the α_7 nicotinic acetylcholine receptor possessing cognition-enhancing properties in vivo. *J. Pharmacol. Exp. Ther.* **2007**, *323*, 294–307.

(14) Sullivan, J. P.; Donnelly-Roberts, D.; Briggs, C. A.; Anderson, D. J.; Gopalakrishnan, M.; Piattoni-Kaplan, M.; Campbell, J. E.; McKenna, D. G.; Molinari, E.; Hettinger, A.-M.; Garvey, D. S.; Wasicak, J. T.; Holladay, M. W.; Williams, M.; Arneric, S. P. A-85380 [3-(2(*S*)-Azetidinylmethoxy) pyridine]: in vitro pharmacological properties of a novel, high affinity $\alpha_4\beta_2$ nicotinic acetylcholine receptor ligand. *Neuropharmacology* **1996**, *35*, 725–734.

(15) *MOE* version 2007.0902; Chemical Computing Group Inc.: Montreal, Quebec, Canada, 2007.

(16) CHARMM version c33b1. Brooks, B. R.; Bruccoleri, R. E.; Olafson, B. D.; States, D. J.; Swaminathan, S.; Karplus, M. CHARMM: A program for macromolecular energy, minimization, and dynamics calculations. *J. Comput. Chem.* **1983**, *4*, 187−217.

(17) Pastor, M.; Cruciani, G.; Clementi, S. Smart region definition: a new way to improve the predictive ability and interpretability of three-dimensional quantitative structure−activity relationships. *J. Med. Chem.* **1997**, *40*, 1455–1464.

(18) ShareGrid project, http://dcs.di.unipmn.it/ (accessed 16th Feb 2009).

JM801060H